Biochimica et Biophysica Acta 1830 (2013) 3447–3453

Contents lists available at SciVerse ScienceDirect

Biochimica et Biophysica Acta

journal homepage: www.elsevier.com/locate/bbagen

Decreased reticuloendothelial system clearance and increased blood half-life and immune cell labeling for nano- and micron-sized superparamagnetic iron-oxide particles upon pre-treatment with Intralipid

Li Liu [a], T. Kevin Hitchens [a], Qing Ye [a], Yijen Wu [a], Brent Barbe [a], Devin E. Prior [a,1], Wendy F. Li [a], Fang-Cheng Yeh [a,b], Lesley M. Foley [a], Daniel J. Bain [c], Chien Ho [a,*]

[a] Pittsburgh NMR Center for Biomedical Research and Department of Biological Sciences, Carnegie Mellon University, Pittsburgh, PA, USA
[b] Department of Biomedical Engineering, Carnegie Mellon University, Pittsburgh, PA, USA
[c] Department of Geology and Planetary Science, University of Pittsburgh, Pittsburgh, PA, USA

ARTICLE INFO

Article history:
Received 10 October 2012
Received in revised form 3 January 2013
Accepted 21 January 2013
Available online 8 February 2013

Keywords:
Nanoparticles
Intralipid
RES clearance
Blood half-life
Labeling of immune cells

ABSTRACT

Background: Superparamagnetic iron-oxide nanoparticles are useful as contrast agents for anatomical, functional and cellular MRI, drug delivery agents, and diagnostic biosensors. Nanoparticles are generally cleared by the reticuloendothelial system (RES), in particular taken up by Kupffer cells in the liver, limiting particle bioavailability and in-vivo applications. Strategies that decrease the RES clearance and prolong the circulation residence time of particles can improve the in-vivo targeting efficiency.
Methods: Intralipid 20.0%, an FDA approved nutritional supplement, was intravenously administered in rats at the clinical dose (2 g/kg) 1 h before intravenous injection of ultra-small superparamagnetic iron-oxide (USPIO) or micron-sized paramagnetic iron-oxide (MPIO) particles. Blood half-life, monocyte labeling efficiency, and particle biodistribution were assessed by magnetic resonance relaxometry, flow cytometry, inductively-coupled plasma MS, and histology.
Results: Pre-treatment with Intralipid resulted in a 3.1-fold increase in USPIO blood half-life and a 2-fold increase in USPIO-labeled monocytes. A 2.5-fold increase in MPIO blood half-life and a 5-fold increase in MPIO-labeled monocytes were observed following Intralipid pre-treatment, with a 3.2-fold increase in mean iron content up to 2.60 pg Fe/monocyte. With Intralipid, there was a 49.2% and 45.1% reduction in liver uptake vs. untreated controls at 48 h for USPIO and MPIO, respectively.
Conclusions: Intralipid pre-treatment significantly decreases initial RES uptake and increases in-vivo circulation and blood monocyte labeling efficiency for nano- and micron-sized superparamagnetic iron-oxide particles.
General significance: Our findings can have broad applications for imaging and drug delivery applications, increasing the bioavailability of nano- and micron-sized particles for target sites other than the liver.

1. Introduction

Iron-oxide particles are useful tools for various biomedical applications including magnetic resonance imaging (MRI) as contrast agents [1–12], targeted drug delivery [13,14], diagnosis [15–17], cell sorting [18,19], and therapy [20,21]. However, in-vivo uses of iron-oxide particles can be hampered by their rapid clearance from circulation by the reticuloendothelial system (RES) [22]. Many studies have reported that the majority of injected iron-oxide particles are taken up by the RES, in particular by the liver Kupffer cells [23,24]. In order to improve the usefulness of these particles for imaging and drug delivery applications, it is essential to minimize the clearance by the RES and improve the in-vivo circulation time.

Non-invasive in-vivo MRI of monocytes/macrophages labeled with iron-oxide particles may lead to a better understanding of the pathogenesis of many diseases, including graft rejection [2,10,25,26], atherosclerotic plaques [27,28], tumors [29,30], abdominal aortic aneurysm [31], renal ischemia [32], Alzheimer's disease [33], etc. Due to the fact that monocytes/macrophages are phagocytes, they can be labeled in

Abbreviations: BN, Brown Norway; FDA, Food and Drug Administration; FITC, fluorescein isothiocyanate; ICP-MS, inductively coupled plasma-mass spectrometry; MPIO, micron-sized superparamagnetic iron-oxide; MRI, magnetic resonance imaging; PBS, phosphate-buffered-saline; ppm, part per million; PEG, polyethylene glycol; r_2, transverse relaxivity; R_2, transverse relaxation rate; RES, reticuloendothelial system; USPIO, ultra-small superparamagnetic iron-oxide

* Corresponding author at: Department of Biological Sciences, Carnegie Mellon University, 4400 Fifth Ave., Pittsburgh, PA 15213, USA. Tel.: +1 412 268 3395; fax: +1 412 268 7083.
E-mail address: chienho@andrew.cmu.edu (C. Ho).
[1] Devin Elizabeth Prior's current address: College of Medicine, Ohio State University, Columbus, OH, USA.

0304-4165/$ – see front matter © 2013 Elsevier B.V. All rights reserved.
http://dx.doi.org/10.1016/j.bbagen.2013.01.021

vivo by a direct injection of suitable iron-oxide particles. Strategies that reduce liver uptake and prolong the circulation residence time of these particles can improve the in-vivo labeling efficiency of monocytes/macrophages and lower the required effective dose.

Many studies have been conducted to decrease the RES clearance and increase the circulation lifetime of iron-oxide particles by modifying particle characteristics, such as the size, charge, surface property, and composition. For example, larger-sized particles are eliminated from bloodstream faster than smaller-sized particles [22]. Neutral and zwitterionic nanoparticles exhibit longer circulation time than negatively and positively charged nanoparticles [34]. In addition, a surface coating of polyethylene glycol (PEG) and modifications of nanoparticles with liposomes can reduce uptake by the RES, thus prolonging their circulation in the bloodstream [35,36]. Modifying the particle characteristics is effective in reducing RES clearance; however, each new modification calls for thorough toxicity and biomechanics studies before any possibility for translation to a clinical setting. Our strategy is to target the RES, and in particular Kupffer cells, to temporarily blunt particle clearance. In this study, we set out to find a U.S. Food and Drug Administration (FDA) approved agent that could achieve this goal.

Intralipid was approved by FDA in 1972 as a source of parenteral nutrition for patients. Intralipid 20.0% is composed of 20% soybean oil, 1.2% egg-yolk phospholipids, and 2.25% glycerol. Kupffer cells in the liver play an important role in the uptake and metabolism of Intralipid [37]. Intralipid infusion has been reported to inhibit RES function by possibly inhibiting peritoneal clearance and impairing the phagocytic activity of Kupffer cells [38]. Our hypothesis is that the clearance of iron-oxide particles by the RES can be reduced by using agents, such as Intralipid, which is also cleared by Kupffer cells and inhibits their phagocytic activities, prior to injection of the particles. In this study, two types of iron-oxide particles were applied to test our hypothesis: nano-sized ultra-small superparamagnetic iron-oxide (USPIO, with particle size ~30 nm in diameter) and micron-sized paramagnetic iron-oxide (MPIO, ~0.9 μm in diameter) particles.

2. Material and methods

2.1. Materials and animals

Intralipid 20.0% was purchased from Fresenius Kabi (Bad Homburg, Germany). "Molday IONC6 Amine" (USPIO-NH_2) particles were purchased from BioPAL (Worcester, MA). MPIO particles coated with polystyrene/divinyl benzene (0.9 μm in size) were obtained from Bangs Laboratories (Fishers, IN). Fluorescein isothiocyanate (FITC) was obtained from Sigma-Aldrich Co. (St. Louis, MO). Phosphate-buffered-saline (PBS) was obtained from Mediatech, Inc. (Manassas, VA). Mouse anti-rat ED1: Alexa Fluor 647 antibody and BUF09 were purchased from AbD SeroTec (Oxford, UK).

Brown Norway (BN; $RT1^n$) rats were purchased from Harlan (Indianapolis, IN). All experiments involving animal subjects were approved by the Institutional Animal Care and Use Committee of Carnegie Mellon University. Animal care was provided in accordance with the Guide for the Care and Use of Laboratory Animals.

2.2. Synthesis and characterization of USPIO-NH_2-FITC

Detailed information on USPIO-NH_2-FITC preparation and characterization is described in Supplementary materials.

2.3. Animal studies

Male BN rats, with body weights between 250 and 280 g, were used in this study. Intralipid 20.0% was administered by intravenous injection at a dose of 2 g/kg (n = 30). PBS was administered to control animals (n = 30). After 1 h, iron-oxide particles were injected intravenously. Two types of iron-oxide particles were tested in this study. Nano-sized USPIO-NH_2-FITC particles were injected at a dose of 4.5 mg Fe/kg body weight (n = 12 for Intralipid pre-treatment group and n = 12 for control group). MPIO particles were injected at a dose of 6 mg Fe/kg body weight (n = 18 for each group). MPIO particles contain a magnetite core as well as a fluorescent dye (Dragon Green) [39]. Blood samples were collected at different time points to determine the blood half-life of the particles and labeling efficiency of monocytes. 48 h post injection of iron-oxide particles, various tissues (liver, spleen, kidney, lung, and heart) were collected for the iron-level determination and histological analysis.

2.4. Biodistribution and iron levels in different tissues

The wet weight of each tissue sample (both USPIO-NH_2 and MPIO treatment groups: n = 6 for Intralipid pre-treatment group and n = 6 for control group) was recorded and 1 mL of tissue homogenate was lypholized in a test tube for 72 h. 1 mL of 6 N HCl was added to each dry tissue sample and the samples were heated overnight in an incubator set at 55 °C. The samples were centrifuged at 500 g for 15 min and the supernatant was collected in a separate test tube. Suitable dilutions of the sample solution were prepared to reach the final concentration in the range of 0.02 to 1 part per million (ppm) with respect to iron. Samples were analyzed for iron concentrations by inductively coupled plasma-mass spectrometry (ICP-MS) (NexION 300X, PerkinElmer Inc., Waltham, MA). Suitable dilutions of standard solutions purchased from CPI International (Santa Rosa, CA) were prepared and a standard curve in the range of 0.02 to 1 ppm Fe was prepared. ^{57}Fe isotope counts were used to determine the Fe content.

The iron levels in different tissues were also determined by transverse relaxation rate (R_2). The R_2 values of tissue samples were measured at 20 MHz using a Bruker Minispec mq20 NMR Analyzer.

2.5. Blood half-life

The R_2 values of blood samples collected at different time points (USPIO-NH_2 treatment group: n = 12 for Intralipid pre-treatment group and n = 12 for control group; MPIO treatment group: n = 18 for each group) were measured using a Bruker Minispec mq20 NMR Analyzer. Blood clearance half-life was determined by fitting the R_2 values to a mono-exponential decay using KaleidaGraph 4.1 (Synergy Software, Reading, PA).

2.6. Flow cytometry

Red blood cells in the blood samples were lysed with ACK lysing buffer (Life Technologies, Carlsbad, CA). Mouse anti-rat ED1: Alexa Fluor 647 antibody was used to label monocytes and macrophages and BUF09 was used as a permeabilization reagent for ED1 detection. Flow cytometry was performed on a FACSVantage (Becton Dickinson, Franklin Lakes, NJ). The data were processed with the use of FlowJo software (TreeStar, Ashland, OR).

2.7. Iron content of labeled-monocytes

48 h following injection of USPIO-NH_2-FITC particles (n = 6 for Intralipid pre-treatment group and n = 6 for control group) and 20 min (n = 6 for each group) or 48 h (n = 6 for each group) after MPIO injection, 7 mL of blood was collected from each rat. Blood monocytes were stained as described above. The USPIO-NH_2-FITC or MPIO-labeled monocytes were sorted with the use of flow cytometry and the numbers of cells were recorded. The collected cells were dissolved in 50 μL of 70% nitric acid. The solutions were then subjected to ICP-MS analysis.

2.8. Histological analysis

Histological examinations were performed by the Transplantation Pathology Laboratory of the University of Pittsburgh Medical Center (Pittsburgh, PA). Perls' Prussian blue staining was conducted for detecting the presence of iron.

2.9. Statistical analysis

The iron levels in different tissues with and without Intralipid pre-treatment were analyzed by Student's *t* test. A p value <0.05 was considered statistically significant.

3. Results

3.1. Synthesis and characterization of USPIO-NH_2-FITC

The conjugation of FITC to USPIO-NH_2 particles increases the hydrodynamic diameter of the particles from 30.2 ± 3.1 nm to 35.5 ± 2.5 nm (Fig. S1). USPIO-NH_2-FITC particles exhibit a similar transverse relaxivity (R_2) value to USPIO particles, which is 81.2 ± 2.5 mM^{-1} s^{-1}, measured at 0.47 T. At pH 7.2, USPIO-NH_2 particles exhibit a zeta potential (ζ) of $+30.2\pm9.1$ mV and USPIO-NH_2-FITC particles exhibit a ζ value of -13.2 ± 7.5 mV in water. Hydrodynamic diameter and zeta potential of the magnetic particles were summarized in Table S1.

3.2. Biodistribution and iron levels in different tissues

Fig. 1 shows the iron concentrations in different tissues as measured by ICP-MS. Tissues from male BN rats, treated with PBS, are used as controls. Greater fractions of nano- or micron-sized iron-oxide particles are found in the liver and spleen, particularly in the liver, than in the heart, kidney, or lung (Fig. 1 and S2). In the liver, the iron concentration increases from 101.0 ± 8.5 (μg/g wet weight) to 189.2 ± 10.5 (μg/g wet weight) 48 h after USPIO-NH_2-FITC injection, while in the spleen, the iron concentration increases from 329.5 ± 55.2 (μg/g wet weight) to 505.6 ± 32.7 (μg/g wet weight) (Fig. 1A). This translates into an ~64.9% uptake in the liver and an ~8.7% uptake in the spleen of the injected iron. Iron concentration also increases 48 h after MPIO injection, from 101.0 ± 8.5 (μg/g wet weight) to 201.9 ± 12.9 (μg/g wet weight) in the liver and from 329.5 ± 55.2 (μg/g wet weight) to 603.0 ± 89.5 (μg/g wet weight) in the spleen (Fig. 1B). Thus, ~55.6% and ~10.2% of the injected MPIO particles are localized in liver and spleen, respectively. Upon pre-treatment with a single dose of Intralipid 20.0% (2 g/kg), the iron content in liver increases to 149.5 ± 19.1 (μg/g wet weight) (Fig. 1A) and 155.9 ± 10.5 (μg/g wet weight) (Fig. 1B) 48 h after the injection of USPIO-NH_2-FITC and MPIO particles, respectively. Thus, the liver uptake of the USPIO-NH_2-FITC particles significantly decreases by 45.1 ± 6.5% and the uptake of MPIO particles significantly decreases by 49.2 ± 5.9%. There is no significant change in uptake in the spleen following Intralipid pre-treatment.

Fig. S2 shows the iron levels in different tissues as measured by the R_2 values. Upon pre-treatment with a single injection of Intralipid, the liver uptake of both USPIO-NH_2-FITC and MPIO particles decreases significantly by 51.2 ± 6.2% and 40.2 ± 5.1%, respectively. In the spleen, a 45.9 ± 11.5% reduction in the uptake of USPIO-NH_2-FITC particles and a 52.2 ± 12.2% reduction in the uptake of MPIO particles are also observed, upon pre-treatment with Intralipid. There is variation in the iron concentrations and the R_2 values of the tissues collected from different animals, which could be due to the heterogeneous distribution of the iron oxide particles in the organ.

Histological examinations of the liver show evidence of iron, as seen with Perls' Prussian blue staining, following the injection of USPIO-NH_2-FITC and MPIO particles (Fig. 2A and C). Upon Intralipid pre-treatment, the presence of iron stained in the liver is significantly decreased (Fig. 2B and D).

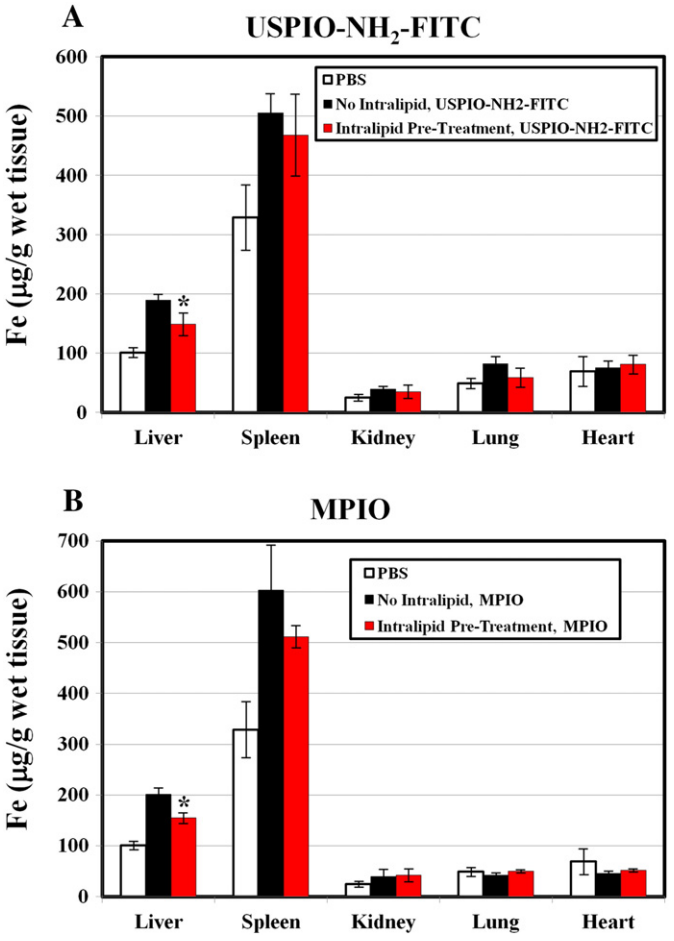

Fig. 1. Changes in the iron levels, as measured by ICP-MS, in different tissues at 48 h following administration of iron-oxide particles upon Intralipid pre-treatment: (A) USPIO-NH_2-FITC particles; and (B) MPIO particles. $^*p<0.01$ compared with iron-oxide particles administrated, but without Intralipid pre-treated samples.

3.3. Blood half-life

Pre-treatment with Intralipid results in a 3- and 2.5-fold increase in the blood half-life of nano- and micron-sized iron-oxide particles, respectively, as determined by the changes in whole blood R_2 values following particle injection. A control experiment was conducted to confirm that Intralipid 20% (diluted 15% v/v) has no effect on the R_2 values for aqueous solutions of USPIO-NH_2-FITC and MPIO particles. The blood half-life of USPIO-NH_2-FITC particles was determined to be 5.1 ± 0.2 min. Upon Intralipid pre-treatment, the half-life increased to 15.9 ± 0.6 min (Fig. 3A). The blood half-life of MPIO particles was 1.3 ± 0.1 min, which is consistent with our previous work [2]. Upon Intralipid pre-treatment, the blood half-life increased to 3.2 ± 0.2 min (Fig. 3B). Thus, Intralipid modulates the pharmacokinetics and prolongs the circulation time of the iron-oxide particles.

3.4. Labeled monocytes found in circulation

Phagocytic immune cells (e.g., monocytes and macrophages) can be labeled in vivo by iron-oxide particles. We have found that pre-treatment with Intralipid significantly enhances the labeling efficiency of blood monocytes/macrophages by nano- and micron-sized iron-oxide particles, as shown by flow cytometry. Fig. 4 shows the kinetics of the appearance of USPIO-NH_2-FITC-labeled and MPIO-labeled monocytes in blood with and without Intralipid pre-treatment. USPIO-NH_2-FITC-labeled monocytes appear in blood slowly after direct i.v. injection of the particles (Fig. 4A). Flow cytometry of blood

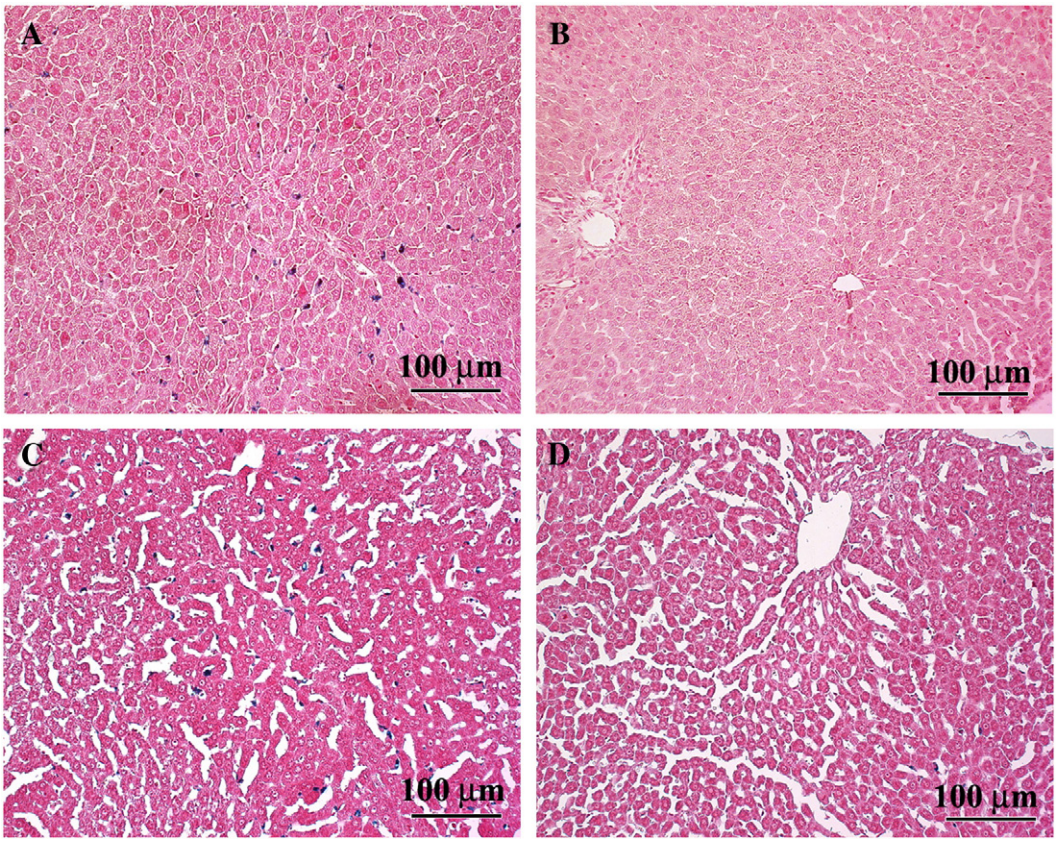

Fig. 2. Histological sections showing the changes in iron levels in liver samples at 48 h following infusion of iron-oxide particles upon Intralipid pre-treatment: (A) USPIO-NH_2-FITC particles; (B) USPIO-NH_2-FITC particles, pre-treatment with Intralipid; (C) MPIO particles; and (D) MPIO particles, pre-treatment with Intralipid. Sections were stained with Perls' Prussian blue and observed under a light microscope at 200× magnification.

samples does not detect USPIO-NH_2-FITC-labeled monocytes after 6 h following particle injection (Fig. 4A upper panel). 24-h post USPIO-NH_2-FITC injection, 5.0 ± 0.9% of the monocytes were labeled. Upon pre-treatment with Intralipid, 5.0 ± 1.1% and 12.2 ± 1.3% of monocytes were labeled with USPIO-NH_2-FITC particles 6- and 24-h post injection, respectively (Fig. 4A lower panel). Fig. 4B shows a summary chart of the flow cytometry data obtained 4-, 6-, 24-, and 48-h post particle injection.

In contrast to the nano-sized particles, MPIO-labeled monocytes are detected in blood shortly after i.v. injection. Fig. 4C upper panel shows that 3.3 ± 0.4% of blood monocytes are labeled with MPIO particles 5 min after particle injection. This labeling efficiency does not change significantly when sampled at 24 h. Upon pre-treatment with Intralipid, 8.5 ± 0.7% of blood monocytes are labeled 5 min after MPIO injection (Fig. 4C lower panel). The labeling efficiency increases to 16.5 ± 0.4% after 20 min and at 24 h, the labeling efficiency is 15.2 ± 1.9%. The plot in Fig. 4D summarizes the labeling results obtained 5-, 10-, 20-min, and 24-hr post MPIO injection.

USPIO-NH_2-FITC- or MPIO-labeled-monocytes were sorted from white blood cells by flow cytometry. About 40,000 labeled-monocytes were harvested from the blood of rats without Intralipid pre-treatment and ~100,000 labeled-monocytes were harvested from Intralipid pre-treated rats. Changes in the iron concentrations in blood monocytes after iron-oxide particle injection upon Intralipid pre-treatment are shown in Table 1. Blood monocytes from male BN rats, treated with PBS, served as controls. Pre-treatment with Intralipid increases the percentage of USPIO-NH_2-FITC-labeled monocytes (Fig. 4A and B), without changing the intracellular iron concentration (~0.2 to 0.3 pg Fe/monocyte). However, pre-treatment with Intralipid causes a three-fold increase in iron concentration of MPIO-labeled monocytes. After 20 min of MPIO injection, but without Intralipid pre-treatment, the intracellular iron concentration in MPIO-labeled monocytes is found to be 0.82 ± 0.12 pg Fe/monocyte, indicating that there are 1 to 2 MPIO particles in each monocyte (~0.5 pg Fe/MPIO particle). Upon Intralipid pre-treatment, the iron concentration increased to 2.60 ± 0.37 pg Fe/monocyte, indicating that there were ~5 MPIO particles in each MPIO-labeled monocyte. 48 h following the MPIO injection, the iron content in MPIO-labeled blood monocytes, without and with pre-treatment with Intralipid, increases to 1.21 ± 0.15 pg Fe/monocyte and 2.92 ± 0.09 pg Fe/monocyte, respectively.

4. Discussion

Many nanocarriers, e.g., iron-oxide particles, micelles, polymers, liposomes, etc., have been used for drug delivery applications [40–44]. An advantage of using iron-oxide particles over other nanocarriers is their dual functionality as an MRI contrast agent as well as drug delivery system. Because the detection of disease pathologies and the effective drug delivery are both critical components of a successful therapy in many disease conditions, iron-oxide particles that can serve both purposes are of high clinical significance. Over the past twenty years, the pharmacokinetics, biodistribution, and target tissue or cell delivery of iron-oxide particles have been widely studied [23,24,45,46]. The injected iron-oxide particles are taken up by the Kupffer cells in the liver, which often contribute to the major loss of the particles in circulation [23,24].

Escaping RES uptake and prolonging the in-vivo circulation of iron-oxide particles can lead to increased uptake in target tissues and cells, which is an important goal in MR imaging, diagnostics, gene and drug delivery as well as other types of therapeutics. The pharmacokinetics and biodistribution of iron-oxide particles depend on their properties, such as size, charge, surface nature, and composition [22,23,34]. In this

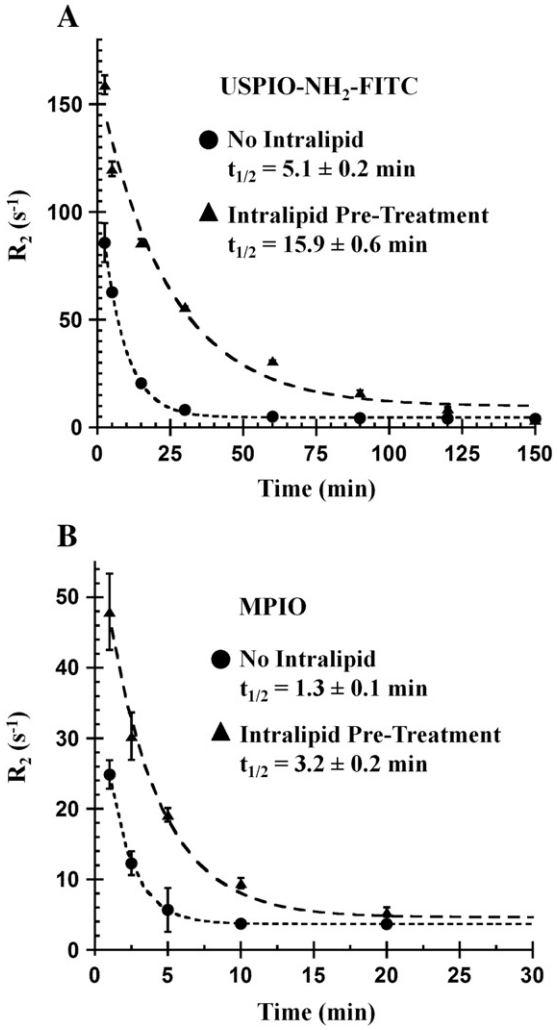

Fig. 3. Changes in blood clearance of iron-oxide particles upon Intralipid pre-treatment: (A) USPIO-NH_2-FITC particles; and (B) MPIO particles.

study, we report the modulation of RES clearance, pharmacokinetics, biodistribution, and immune-cell uptake of iron-oxide particles by pre-treatment with Intralipid.

Phagocytic activity of the RES and the RES blockade has been studied for over 50 years [38,47,48]. Various oil emulsions have been shown to inhibit or stimulate the phagocytic activity of RES, depending on the physical or chemical properties of the oil emulsions [48]. We believe that the administration routes of the oil emulsions and the time courses of the measurements are also critical issues. In this study, Intralipid 20.0% (2 g/kg) was administered by intravenous injection 1 h before the infusion of iron-oxide particles. This acute Intralipid treatment should not change the baseline iron concentration in the organs. A 45.1 ± 6.5% reduction in liver uptake of USPIO-NH_2-FITC particles and a 49.2 ± 5.9% reduction in liver uptake of MPIO particles have been observed (Figs. 1, 2, and S2). The RES plays an important role in the uptake and metabolism of Intralipid, and the blood half-life of Intralipid 20.0% administered by intravenous bolus in rats is 8.7 ± 3.0 min [37,49]. To achieve the greatest reduction in RES uptake of the iron-oxide particles, the administration routes and the time courses will have to be optimized in future studies.

Hepatic Kupffer cells are responsible for ~90% of the total phagocytic capacity that is involved in maintaining homeostasis in circulation [50]. When Kupffer cell activity needs to be reduced, e.g., in order to enhance the efficiency of gene delivery, clodronate liposomes have been applied to deplete Kupffer cells in the liver [51]. However, the depletion effects of clodronate liposomes should be transient, but the reappearance of Kupffer cells could take up to one week [50]. The findings in this study show that Intralipid provides a safer way to temporarily inhibit Kupffer cell activity and improve therapeutic efficacy.

Pre-treatment with Intralipid produces a 3-fold increase in the blood half-life of USPIO-NH_2-FITC particles (Fig. 3A) and a 2.5-fold increase in the blood half-life of MPIO particles (Fig. 3B). Therefore, the nano- and micron-sized iron-oxide particles have an extended blood circulation time, allowing more time for accumulation at target organs and tissues. Of note, it is also interesting to see that the USPIO-NH_2-FITC particles synthesized in our laboratory exhibited a shorter half-life of 5.1 ± 0.2 min, when compared to the neutral USPIO particle, "Molday ION" (BioPAL, Worcester, MA), which has a blood half-life of several hours [52]. Our findings are consistent with the report that neutral and zwitterionic nanoparticles possess longer half-lives than positively or negatively charged nanoparticles [34].

In-vivo labeling of monocytes/macrophages with iron-oxide particles for MRI has been applied to image many disease conditions, such as graft rejection, atherosclerotic plaques, tumors, abdominal aortic aneurysm, renal ischemia, and Alzheimer's disease [2,10,25,27–33]. Our laboratory has been able to monitor the infiltration of macrophages labeled with USPIO or MPIO particles at rejecting kidneys, hearts, and lungs in our rat models for organ transplantation using the in-vivo labeling procedure [2,10,25,53,54]. We have found that a single MPIO-labeled macrophage can be detected by MRI [2,10]. This is due to the large iron core sizes of MPIO particles (0.5 to several μm) and the local magnetic-field gradient that iron-oxide particles can generate, which can be up to 50 times its radius [10,55,56]. This is why the ability to increase the loading of the monocytes/macrophages is so important, particularly for in-vivo imaging. Escaping the initial RES clearance and prolonging the in-vivo circulation enable increased labeling efficiency of monocytes/macrophages by the iron-oxide particles. Without Intralipid pre-treatment, our results reveal that only about 3 to 5% of blood monocytes are labeled with MPIO particles (Fig. 4C and D) and the intracellular iron concentration is 0.82 ± 0.12 pg Fe/monocyte 20 min after the MPIO injection (Table 1). Upon the Intralipid pre-treatment, the monocyte labeling efficiency increases to about 15% and the iron content increases to 2.60 ± 0.37 pg Fe/monocyte. Pre-treatment with Intralipid also produces a 2-fold increase in monocyte labeling efficiency with nano-sized iron-oxide particles (Fig. 4A and B). These findings are important because our approach can increase the labeling efficiency of monocytes/macrophages with nano- to micron-sized iron-oxide particles, and therefore the dose of the contrast agent needed for in-vivo cell tracking and imaging experiments can be minimized.

An interesting observation in this study is that the kinetics of the appearance of USPIO-NH_2-FITC-labeled and MPIO-labeled monocytes in blood is different following direct i.v. injection of the particles (Fig. 4). MPIO-labeled cells are detected in blood at 5 min after injection, whereas USPIO-labeled cells are not observed in significant numbers until 24 h, or 6 h with Intralipid pre-treatment. Rapid labeling for MPIO particles suggests that the circulating monocytes take up MPIO particles via endocytosis. The slow appearance of USPIO-NH_2-FITC-labeled monocytes in blood indicates that the labeling of monocytes/macrophages may occur in locations other than the blood, possibly in the spleen and/or bone marrow, and that the labeled monocytes/macrophages migrate to the blood after 24 h. Recently, an important question has been raised: when and where do the monocytes/macrophages acquire the iron-oxide-particle-label [57]? Our results suggest that labeling of monocytes/macrophages by different iron-oxide particles might follow different pathways, and depending on the particles and/or other conditions taking place alternatively in circulation and/or in organs, such as the spleen and bone marrow.

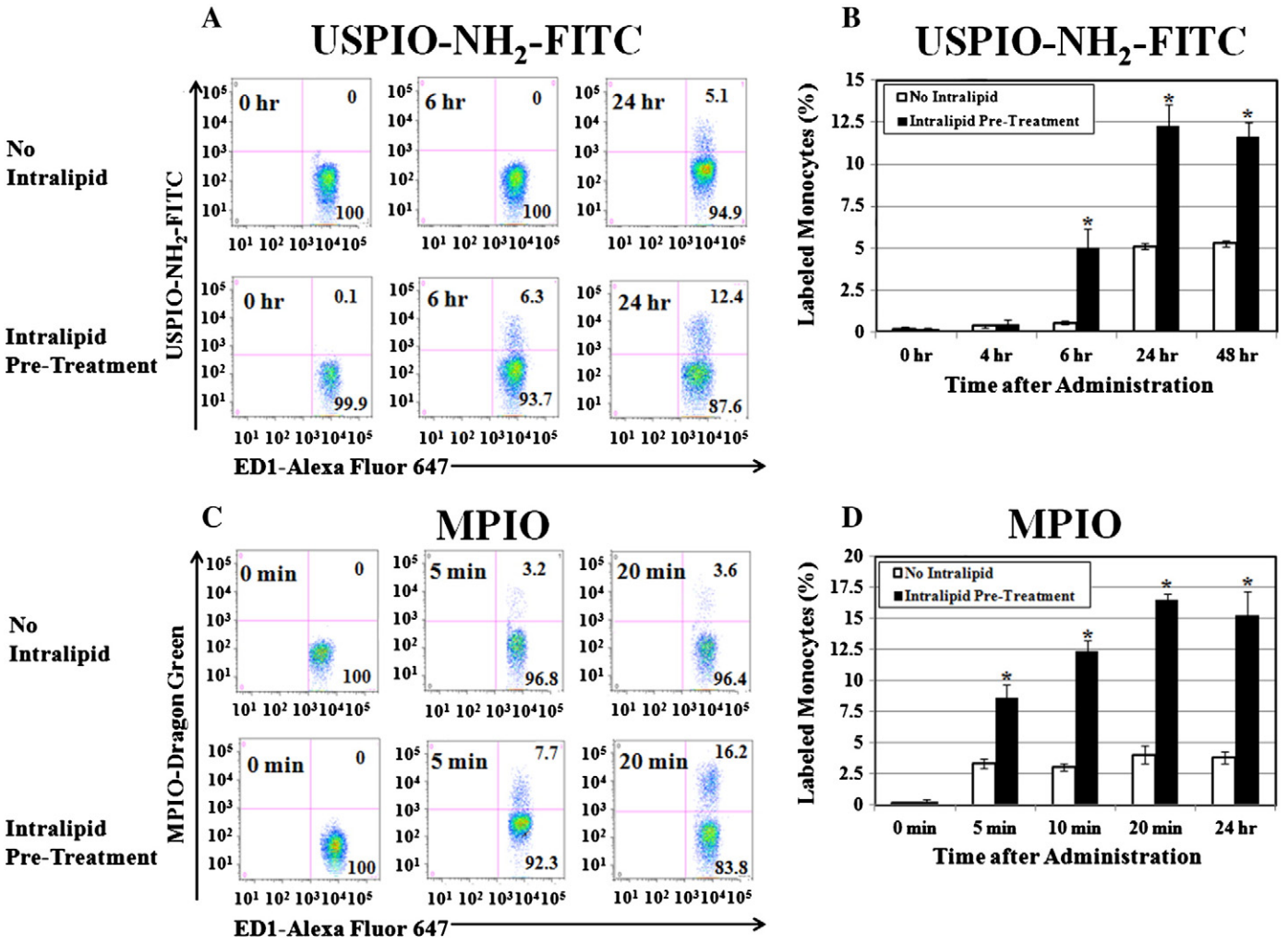

Fig. 4. Changes in blood monocyte labeling by iron-oxide particles upon Intralipid pre-treatment. Representative flow cytometry dot plots showing the kinetics of blood monocyte labeled by (A) USPIO-NH_2-FITC particles and (C) MPIO particles upon Intralipid pre-treatment. (B) and (D) are summary charts of the data shown in (A) and (C), respectively. $^*p<0.01$ compared with iron-oxide particles administrated, but without Intralipid pre-treated samples.

In conclusion, we have found that pre-treatment with Intralipid, an FDA approved fat supplement, can result in an ~50% decrease in liver uptake and an ~3-fold increase in blood half-life of nano- and micron-sized iron-oxide particles, resulting in a 2- to 5-fold increase in the labeling efficiency of monocytes/macrophages in the peripheral blood. Our results suggest that Intralipid can affect the pharmacokinetics of nano- and micron-sized particles, thus improving drug targeting and imaging applications of these particles for targets other than the liver.

Table 1
Effects of Intralipid on the iron concentrations in blood monocytes after injection of iron-oxide particles.

Pre-treatment	Iron-oxide particles	Duration after particle injection	Iron concentration (pg Fe/monocyte)
PBS	PBS	20 min	0.04 ± 0.02
PBS	USPIO-NH2-FITC	48 h	0.28 ± 0.07
Intralipid	USPIO-NH2-FITC	48 h	0.22 ± 0.07
PBS	MPIO	20 min	0.82 ± 0.12
Intralipid	MPIO	20 min	2.60 ± 0.37
PBS	MPIO	48 h	1.21 ± 0.15
Intralipid	MPIO	48 h	2.92 ± 0.09

Acknowledgements

This work is supported by research grants from the National Institutes of Health (R01HL-081349 and P41EB-001977 to C. H.) and a Postdoctoral Fellowship awarded by the American Heart Association (10POST3010016 to L. L.).

We thank Ms. Lily Chen for assistance with immune cell labeling experiments, Mr. Yehuda Creeger for assistance in the flow cytometry analysis, and Ms. Lisa McGaw for taking care of the animals.

Appendix A. Supplementary data

Supplementary data to this article can be found online at http://dx.doi.org/10.1016/j.bbagen.2013.01.021.

References

[1] C. Ho, T.K. Hitchens, A non-invasive approach to detecting organ rejection by MRI: monitoring the accumulation of immune cells at the transplanted organ, Curr. Pharm. Biotechnol. 5 (2004) 551–566.
[2] Q. Ye, Y.L. Wu, L.M. Foley, T.K. Hitchens, D.F. Eytan, H. Shirwan, C. Ho, Longitudinal tracking of recipient macrophages in a rat chronic cardiac allograft rejection model with noninvasive magnetic resonance imaging using micrometer-sized paramagnetic iron oxide particles, Circulation 118 (2008) 149–156.
[3] C.L. Chen, H. Zhang, Q. Ye, W.Y. Hsieh, T.K. Hitchens, H.H. Shen, L. Liu, Y.J. Wu, L.M. Foley, S.J. Wang, C. Ho, A new nano-sized iron oxide particle with high sensitivity for cellular magnetic resonance imaging, Mol. Imaging Biol. 13 (2011) 825–839.

[4] M.S. Thu, L.H. Bryant, T. Coppola, E.K. Jordan, M.D. Budde, B.K. Lewis, A. Chaudhry, J. Ren, N.R. Varma, A.S. Arbab, J.A. Frank, Self-assembling nanocomplexes by combining ferumoxytol, heparin and protamine for cell tracking by magnetic resonance imaging, Nat. Med. 18 (2012) 463–467.
[5] E.M. Shapiro, S. Skrtic, K. Sharer, J.M. Hill, C.E. Dunbar, A.P. Koretsky, MRI detection of single particles for cellular imaging, Proc. Natl. Acad. Sci. U.S.A. 101 (2004) 10901–10906.
[6] D.L. Kraitchman, D.A. Kedziorek, J.W. Bulte, MR imaging of transplanted stem cells in myocardial infarction, Methods Mol. Biol. 680 (2011) 141–152.
[7] J.P. Sumner, E.M. Shapiro, D. Maric, R. Conroy, A.P. Koretsky, In vivo labeling of adult neural progenitors for MRI with micron sized particles of iron oxide: quantification of labeled cell phenotype, NeuroImage 44 (2009) 671–678.
[8] D. Granot, D. Scheinost, E.A. Markakis, X. Papademetris, E.M. Shapiro, Serial monitoring of endogenous neuroblast migration by cellular MRI, NeuroImage 57 (2011) 817–824.
[9] L. Liu, Q. Ye, Y. Wu, W.Y. Hsieh, C.L. Chen, H.H. Shen, S.J. Wang, H. Zhang, T.K. Hitchens, C. Ho, Tracking T-cells in vivo with a new nano-sized MRI contrast agent, Nanomedicine 8 (2012) 1345–1354.
[10] Y.L. Wu, Q. Ye, L.M. Foley, T.K. Hitchens, K. Sato, J.B. Williams, C. Ho, In situ labeling of immune cells with iron oxide particles: an approach to detect organ rejection by cellular MRI, Proc. Natl. Acad. Sci. U. S. A. 103 (2006) 1852–1857.
[11] D.L. Thorek, A. Tsourkas, Size, charge and concentration dependent uptake of iron oxide particles by non-phagocytic cells, Biomaterials 29 (2008) 3583–3590.
[12] S.H. Crayton, A. Tsourkas, pH-titratable superparamagnetic iron oxide for improved nanoparticle accumulation in acidic tumor microenvironments, ACS Nano 5 (2011) 9592–9601.
[13] A.Z. Wang, F. Gu, L. Zhang, J.M. Chan, A. Radovic-Moreno, M.R. Shaikh, O.C. Farokhzad, Biofunctionalized targeted nanoparticles for therapeutic applications, Expert. Opin. Biol. Ther. 8 (2008) 1063–1070.
[14] F.M. Kievit, M. Zhang, Surface engineering of iron oxide nanoparticles for targeted cancer therapy, Acc. Chem. Res. 44 (2011) 853–862.
[15] C. del Frate, M. Bazzocchi, K.J. Mortele, C. Zuiani, V. Londero, G. Como, R. Zanardi, P.R. Ros, Detection of liver metastases: comparison of gadobenate dimeglumine-enhanced and ferumoxides-enhanced MR imaging examinations, Radiology 225 (2002) 766–772.
[16] H. Prosch, E. Oschatz, E. Pertusini, G. Mostbeck, Diagnosis of thoracic splenosis by ferumoxides-enhanced magnetic resonance imaging, J. Thorac. Imaging 21 (2006) 235–237.
[17] Y. Asahina, N. Izumi, M. Uchihara, O. Noguchi, K. Ueda, K. Inoue, Y. Nishimura, K. Tsuchiya, K. Hamano, J. Itakura, Y. Himeno, M. Koike, S. Miyake, Assessment of Kupffer cells by ferumoxides-enhanced MR imaging is beneficial for diagnosis of hepatocellular carcinoma: comparison of pathological diagnosis and perfusion patterns assessed by CT hepatic arteriography and CT arterioportography, Hepatol. Res. 27 (2003) 196–204.
[18] J.H. Clement, M. Schwalbe, N. Buske, K. Wagner, M. Schnabelrauch, P. Gornert, K.O. Kliche, K. Pachmann, W. Weitschies, K. Hoffken, Differential interaction of magnetic nanoparticles with tumor cells and peripheral blood cells, J. Cancer Res. Clin. Oncol. 132 (2006) 287–292.
[19] H. Xu, Z.P. Aguilar, L. Yang, M. Kuang, H. Duan, Y. Xiong, H. Wei, A. Wang, Antibody conjugated magnetic iron oxide nanoparticles for cancer cell separation in fresh whole blood, Biomaterials 32 (2011) 9758–9765.
[20] N.H. Cho, T.C. Cheong, J.H. Min, J.H. Wu, S.J. Lee, D. Kim, J.S. Yang, S. Kim, Y.K. Kim, S.Y. Seong, A multifunctional core-shell nanoparticle for dendritic cell-based cancer immunotherapy, Nat. Nanotechnol. 6 (2011) 675–682.
[21] A. Ito, K. Tanaka, K. Kondo, M. Shinkai, H. Honda, K. Matsumoto, T. Saida, T. Kobayashi, Tumor regression by combined immunotherapy and hyperthermia using magnetic nanoparticles in an experimental subcutaneous murine melanoma, Cancer Sci. 94 (2003) 308–313.
[22] Tobias Neuberger, Bernhard Schöpf, Heinrich Hofmann, Margarete Hofmann, Brigitte von Rechenberg, Superparamagnetic nanoparticles for biomedical applications: possibilities and limitations of a new drug delivery system, J. Magn. Magn. Mater. 293 (2005) 483–496.
[23] C. Chouly, D. Pouliquen, I. Lucet, J.J. Jeune, P. Jallet, Development of superparamagnetic nanoparticles for MRI: effect of particle size, charge and surface nature on biodistribution, J. Microencapsul. 13 (1996) 245–255.
[24] E. Okon, D. Pouliquen, P. Okon, Z.V. Kovaleva, T.P. Stepanova, S.G. Lavit, B.N. Kudryavtsev, P. Jallet, Biodegradation of magnetite dextran nanoparticles in the rat. A histologic and biophysical study, Lab. Invest. 71 (1994) 895–903.
[25] Y.L. Wu, Q. Ye, K. Sato, L.M. Foley, T.K. Hitchens, C. Ho, Noninvasive evaluation of cardiac allograft rejection by cellular and functional cardiac magnetic resonance, JACC Cardiovasc. Imaging 2 (2009) 731–741.
[26] Y.L. Wu, Q. Ye, C. Ho, Cellular and functional imaging of cardiac transplant rejection, Curr. Cardiovasc. Imaging Rep. 4 (2011) 26–50.
[27] T.Y. Tang, K.H. Muller, M.J. Graves, Z.Y. Li, S.R. Walsh, V. Young, U. Sadat, S.P. Howarth, J.H. Gillard, Iron oxide particles for atheroma imaging, Arterioscler. Thromb. Vasc. Biol. 29 (2009) 1001–1008.
[28] C. Tu, T.S.C. Ng, H.K. Sohi, H.A. Palko, A. House, R.E. Jacobs, A.Y. Louie, Receptor-targeted iron oxide nanoparticles for molecular MR imaging of inflamed atherosclerotic plaques, Biomaterials 32 (2011) 7209–7216.
[29] H.E. Daldrup-Link, D. Golovko, B. Ruffell, D.G. Denardo, R. Castaneda, C. Ansari, J. Rao, G.A. Tikhomirov, M.F. Wendland, C. Corot, L.M. Coussens, MRI of tumor-associated macrophages with clinically applicable iron oxide nanoparticles, Clin. Cancer Res. 17 (2011) 5695–5704.
[30] Y.-Y.I. Shih, Y.-H. Hsu, T.Q. Duong, S.-S. Lin, K.-P.N. Chow, C. Chang, Longitudinal study of tumor-associated macrophages during tumor expansion using MRI, NMR Biomed. 24 (2011) 1353–1360.
[31] N. Miyama, M.M. Dua, G.M. Schultz, H. Kosuge, M. Terashima, L.J. Pisani, R.L. Dalman, M.V. McConnell, Bioluminescence and magnetic resonance imaging of macrophage homing to experimental abdominal aortic aneurysms, Mol. Imaging 11 (2012) 126–134.
[32] S.K. Jo, X. Hu, H. Kobayashi, M. Lizak, T. Miyaji, A. Koretsky, R.A. Star, Detection of inflammation following renal ischemia by magnetic resonance imaging, Kidney Int. 64 (2003) 43–51.
[33] N. Beckmann, C. Gerard, D. Abramowski, C. Cannet, M. Staufenbiel, Noninvasive magnetic resonance imaging detection of cerebral amyloid angiopathy-related microvascular alterations using superparamagnetic iron oxide particles in APP transgenic mouse models of Alzheimer's disease: application to passive Abeta immunotherapy, J. Neurosci. Off. J. Soc. Neurosci. 31 (2011) 1023–1031.
[34] R.R. Arvizo, O.R. Miranda, D.F. Moyano, C.A. Walden, K. Giri, R. Bhattacharya, J.D. Robertson, V.M. Rotello, J.M. Reid, P. Mukherjee, Modulating pharmacokinetics, tumor uptake and biodistribution by engineered nanoparticles, PLoS One 6 (2011) e24374.
[35] S. Maesaki, Drug delivery system of anti-fungal and parasitic agents, Curr. Pharm. Des. 8 (2002) 433–440.
[36] B. Romberg, W.E. Hennink, G. Storm, Sheddable coatings for long-circulating nanoparticles, Pharm. Res. 25 (2008) 55–71.
[37] S. Vilaro, M. Llobera, Uptake and metabolism of Intralipid by rat liver: an electron-microscopic study, J. Nutr. 118 (1988) 932–940.
[38] K.M. Nugent, Intralipid effects on reticuloendothelial function, J. Leukoc. Biol. 36 (1984) 123–132.
[39] http://www.bangslabs.com/sites/default/files/bangs/docs/pdf/PDS_731.pdf.
[40] E. Blanco, A. Hsiao, A.P. Mann, M.G. Landry, F. Meric-Bernstam, M. Ferrari, Nanomedicine in cancer therapy: innovative trends and prospects, Cancer Sci. 102 (2011) 1247–1252.
[41] Y. Malam, M. Loizidou, A.M. Seifalian, Liposomes and nanoparticles: nanosized vehicles for drug delivery in cancer, Trends Pharmacol. Sci. 30 (2009) 592–599.
[42] S. Bhaskar, F. Tian, T. Stoeger, W. Kreyling, J.M. de la Fuente, V. Grazu, P. Borm, G. Estrada, V. Ntziachristos, D. Razansky, Multifunctional nanocarriers for diagnostics, drug delivery and targeted treatment across blood–brain barrier: perspectives on tracking and neuroimaging, Part. Fibre Toxicol. 7 (2010) 3.
[43] M. Talelli, K. Morita, C.J. Rijcken, R.W. Aben, T. Lammers, H.W. Scheeren, C.F. van Nostrum, G. Storm, W.E. Hennink, Synthesis and characterization of biodegradable and thermosensitive polymeric micelles with covalently bound doxorubicin-glucuronide prodrug via click chemistry, Bioconjug. Chem. 22 (2011) 2519–2530.
[44] A. Qi, P. Chan, J. Ho, A. Rajapaksa, J. Friend, L. Yeo, Template-free synthesis and encapsulation technique for layer-by-layer polymer nanocarrier fabrication, ACS Nano 5 (2011) 9583–9591.
[45] T.K. Jain, M.K. Reddy, M.A. Morales, D.L. Leslie-Pelecky, V. Labhasetwar, Biodistribution, clearance, and biocompatibility of iron oxide magnetic nanoparticles in rats, Mol. Pharm. 5 (2008) 316–327.
[46] L.M. Lacava, Z.G. Lacava, M.F. Da Silva, O. Silva, S.B. Chaves, R.B. Azevedo, F. Pelegrini, C. Gansau, N. Buske, D. Sabolovic, P.C. Morais, Magnetic resonance of a dextran-coated magnetic fluid intravenously administered in mice, Biophys. J. 80 (2001) 2483–2486.
[47] I.M. Murray, The mechanism of blockade of the reticuloendothelial system, J. Exp. Med. 117 (1963) 139–147.
[48] B. Pipy, D. Gaillard, R. Derache, [Effect of the quality of various vegetable oil emulsions on phagocytotic activity of the reticuloendothelial system in the rat]. Influence de la qualite de diverses emulsions d'huiles vegetales sur l'activite phagocytaire du systeme reticuloendothelial du rat, Ann. Nutr. Aliment. 29 (1975) 271–284.
[49] I. Fraser, H. Pearson, V. Bowry, P.R. Bell, The intravenous Intralipid tolerance test, J. Leukoc. Biol. 36 (1984) 647–649.
[50] N. van Rooijen, E. van Kesteren-Hendrikx, Clodronate liposomes: perspectives in research and therapeutics, J. Liposome Res. 12 (2002) 81–94.
[51] K. Schughart, R. Bischoff, D.A. Hadji, O. Boussif, F. Perraud, N. Accart, U.B. Rasmussen, A. Pavirani, N. van Rooijen, H.V. Kolbe, Effect of liposome-encapsulated clodronate pretreatment on synthetic vector-mediated gene expression in mice, Gene Ther. 6 (1999) 448–453.
[52] http://www.biopal.com/Molday%20ION.htm.
[53] D. Yang, Q. Ye, M. Williams, Y. Sun, T.C. Hu, D.S. Williams, J.M. Moura, C. Ho, USPIO-enhanced dynamic MRI: evaluation of normal and transplanted rat kidneys, Magn. Reson. Med. 46 (2001) 1152–1163.
[54] Q. Ye, D. Yang, M. Williams, D.S. Williams, C. Pluempitiwiriyawej, J.M. Moura, C. Ho, In vivo detection of acute rat renal allograft rejection by MRI with USPIO particles, Kidney Int. 61 (2002) 1124–1135.
[55] P. Lauterbur, M. Bernardo, M. Menonca Dias, L. Hedges, Microscopic NMR imaging of the magnetic field around magnetic particles, Proceedings of the Society for Magnetic Resonance in Medicine, 5th Annual Meeting, 1986, pp. 229–230.
[56] S.J. Dodd, M. Williams, J.P. Suhan, D.S. Williams, A.P. Koretsky, C. Ho, Detection of single mammalian cells by high-resolution magnetic resonance imaging, Biophys. J. 76 (1999) 103–109.
[57] K.S. Tang, B. Hann, E.M. Shapiro, On the use of micron-sized iron oxide particles (MPIOS) to label resting monocytes in bone marrow, Mol. Imaging Biol. 13 (2011) 819–824.